Influence the Addition (SiO$_2$) Nanoparticles on Optical Properties for Methylene Blue Dye

Maha Hassan Noory[1*], Zaid A.Hasan[2]

Abstract

Thin films from methylene blue dye dopant with silicon oxide nanoparticles (semiconducting) with percentages (0, 0.01, 0.03 and 0.05%) with a thickness of 0.001 nm, had been prepared in this research. The effect of silicon oxide impurities in methylene blue dye on the optical properties (absorption, absorbance coefficient, transmittance, energy band-gap for the forbidden and permissible electronic transitions, refractive index, extinction coefficient, dielectric constant with its real and imaginary particles, and photoconductivity) was investigated by Spectrophotometer route in the visible range 400-800 nm. Show that studying of pure and dopants samples with previous ratios increasing of absorption coefficient with increasing the doped ratios, in addition the optical conductivity, as for the values of the band gap for forbidden and permissible transitions, they decreased with the increase by the dopants percentage.

Introduction

Semiconducting oxide nanoparticles have received wide interest in many applications such as catalysts, sensors and others. (Jassim M et al, 2013; Fernandez et al, 2011; Zaid, 2021; Zaid, 2019), It is known that mixing metal oxides in inert support materials prevents caking in addition to improving its properties and thermal stability. From another point of view, these compounds attracted clear interest on solid silica deposition with metallic nanoparticles to know many of their chemical and physical properties that are difficult to obtain in their natural form (Srivastava et al, 2014; Liu et al 2010). In many studies, SiO2 films have been widely used in electronic devices due to their important properties in terms of resistance to corrosion and reflection constant, as well as thermal and electrical insulation (Yang et al, 1997; Maekawa. Et al, 1994; Ardalan et al, 2017; Park et al, 2012; Ghazarya et al 2019). In addition, its uses are in electronic devices, displays, and energy-saving windows (Sietsma et al, 2007; Yadav. Et al, 2010; TAN. Et al, 2008). Its value varies according to the method of preparation, as you put its value from 1.39ev to 3.88ev (Vishwakarma. Et al, 2013; Ghobadi et al, 2020). Also, these films are transparent in the infrared field, as they are transparent with a high transmittance coefficient up to ~70% (Suthan et al, 2010) Also, these oxides are characterized by a high permeability in the visible field and a good conductivity close to that of metals (Suthan et al, 2010) The organic and analytical dyes are among the most important dyes that are used in many industries in terms of their participation in the textile, furniture and paint industries, but it poses a threat to the environment and green chemistry.

Corresponding author: Maha Hassan Noory

Address: [1*]University of Babylon, Iraq; [2]University of Babylon, Iraq.

[2]E-mail: zaid.shimary@yahoo.com; pure.zaid.adul@uobabylon.edu.iq

Because it is toxic and among the chemical compounds that lead to cancer (Stylidi. et al, 2003; Zhong et al, 2012), and among these colors, methylene blue is a good dye in terms of solubility as it has solubility in several organic and inorganic solvents in addition to water, and this distinguishes it from the rest of the dyes from the point of view of its entry into the chemical composition as an environmentally friendly dye (Gholami et al, 2015) and from the above, given the use of methylene blue in scientific research laboratories, this was used in our research.

Experimental

i. 25 ml of chloroform alcohol was poured into a 100 ml volumetric flask with the addition 0.2g methylene blue dye. The vessel is placed in a rotating device that operates at a frequency of 1.2 kHz, then the agitator is placed inside this vessel to stir the solution until complete dissolution for about 30 minutes at a temperature of 150°C.

ii. After complete dissolution, the solution was drip onto a glass slide to obtain a thin plate (drip and wipe method).

iii. Same steps 1 and 2 are repeated with the addition of 2% of nanoparticles until complete dissolution and then drop it on a glass slide.

iv. The same steps are repeated 1, 2 and 3 with a change in the weight ratios of the nanoparticles to obtain other dyes.

v. Leave dyes to dry completely.

Results

This research aims to study the nonlinear optics of methylene blue dye doped with nanoparticles of SiO₂ at different weights (Pure, 0.01, 0.03 and 0.05 %). The essence of our optical study lies in determining the transmittance and absorption coefficient, thus energy band gap, then we calculate the real and imaginary part of the dielectric constant, also the damping coefficient, the refractive index, and finally the optical conductivity of the prepared samples, through measurable quantities.

Optical transmittance T ($T = \frac{I_T}{I_0}$ where I_T is the transmissive intensity, I_0 is the incoming quantum intensity) and the reflectivity R ($R = \frac{I_R}{I_0}$ where I_R is the reflected intensity, I_0 is the incoming quantum intensity. A study of transmittance and reflectivity in the case of normal rosette with the existing

spectrophotometer Model Spectrophotometer JASCO (UV-570) Dual Action it measures in the range of wavelengths (400-800 nm).

Transmittance T

The figure 1 shows the transmittance spectra of the prepared samples.
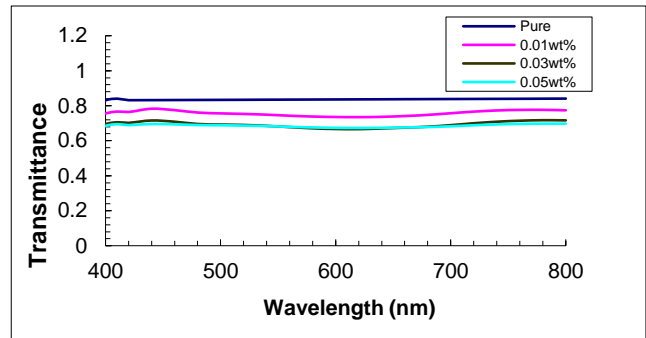

Fig. 1. Changes of transmittance in terms of wavelength λ(nm)

The previous figure for the studied samples shows that the transmittance spectrum of the pure sample is higher than that of the doped samples and at the percentage of doping 0.03 and 0.05 the transmittance spectrum is almost the same, with a clear decrease in the similar spectra at 600 nm almost.

Absorption A

The formula. 1 shows the conservation law of energy (Zaid A. Hasan, 2021); (Jaaraj et al, 2002):

$$A+R+T=1 \qquad (1)$$

where A (Absorbance) which is the loss of light energy within the sample before the light enters it. We infer from this formula, the behavior of the absorption spectrum through the absorbance

$$A= 1-(R+T) \qquad (2)$$

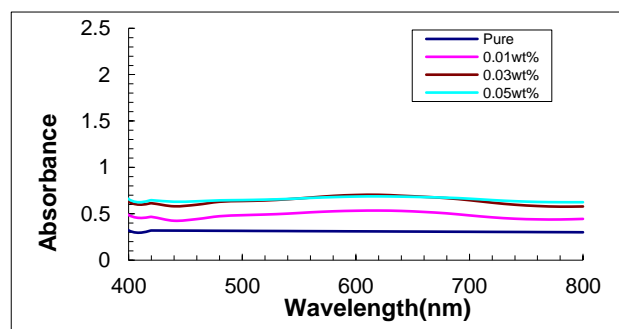The study of the change the sum (R+T), shows us the absorption behavior and absorption range in the samples.

Fig. 2. The absorbance changes as a function of wavelength λ(nm)

It shows from that absorbance spectra is opposite to the optical transmittance, as the absorption spectrum of the pure sample is the lowest possible, Then the absorbance increases when increase in doped ratios. Likewise, we find that the absorbance spectra at the doped ratios 0.03 and 0.05 they are as high as possible and are almost similar at these two ratios and the highest absorption peak at the wavelength 600 nm approx. We find that the absorption spectrum increases slightly from 400 to 650 nm and then begins to decrease to 800 nm. This loss (optical wave extinction), which may be due to several factors in absorption and scattering caused by the remains of unreactive molecules.

Absorption Coefficient α

Optical transmittance, spectroscopic measurements T shown in Figure.1 were used to calculate the absorption coefficient of samples from the following formula (Zaid A. Hasan; Venkatachalam et al, 2007):

$$\alpha = \frac{1}{d} ln(\frac{1}{T}), \text{ or: } \alpha = \frac{1}{d} 2.303 \, log(\frac{1}{T}) \quad (3)$$

Where T: Transmittance, d: thickness. This is based on Lambert's law (Venkatachalam et al, 2007), which defines the formula: $I_t = I e^{-\alpha d}$ ......(4), where I is the intensity of light incident on sample, I_t is the intensity of light transmission through it and represents the magnitude $D = log(\frac{1}{T})$ here it is optical density
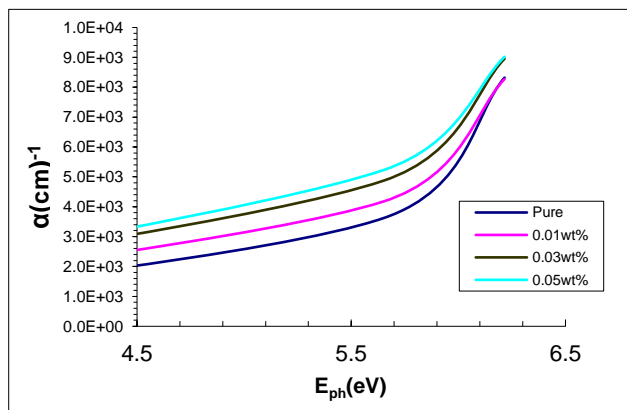

Fig. 3. Variations of absorption coefficient in terms of photon energy

We note that values of the absorption coefficient increase with increase in doping ratios, especially at high energies, we also note that the change in the absorption coefficient with the energy of the photon is slightly at low energies and then changes rapidly and significantly near the edge of optical absorption. As it is clear from all the curves that there is an absorption region $\alpha < 10^4 \, cm^{-1}$ and this is likely not to occur direct electronic transitions, as we note

that the absorption edges are slightly shifted towards low photon energies and this effect is called (Burstien-Moss) and the reason for this is due to the generation of donor levels within the band gap near the conductivity band, this led to the absorption of low-energy photons, and consequently, a clear increase in the values of the absorption coefficient (Tariq, 2010).

Calculate of the Width of Energy Band Gap E_g

The energy band gap has been set for the permissible and forbidden direct electronic transfers, the absorption coefficient α for the two transitions can be calculated from the following formula (Habubi et al, 2002):

$$(\alpha h\upsilon = B(h\upsilon - E_g)^r \quad (5)$$

Where: υ is the frequency of incident light, h: is Planck's constant, B: is a constant depends on the properties of valence and transmissive bands, $h\upsilon$: the absorbed photovoltaic energy. E_g: energy gap, α: absorption coefficient. The value of the exponent (r) depends on nature of transitions. In the permissible direct transfers, its value is 1/2, and formula (5) takes the form: $(\alpha h\upsilon)^2 = B^2(h\upsilon - E_g)$.

In the case of forbidden direct transitions, its value is 2/3, and formula (4) takes the form: $(\alpha h\upsilon)^{3/2} = B^{3/2} (h\upsilon - E_g)$, and the value of the energy gap E_g corresponding to direct electronic transitions are determined graphically from the graph of the graph of $(\alpha h\upsilon)^m$ changes in terms of $(h\upsilon)$ Then the best and farthest linear part of the curve is taken and plotted as a straight line tangent to it.

So that an extended intersection of this tangent with the horizontal axis $(h\upsilon)$ corresponds to the value of the energy gap E_g, and becomes $(\alpha h\upsilon)^m = 0$. Figures. (4), (5) represents the energy gap of the films in permissible and forbidden direct electronic transitions.
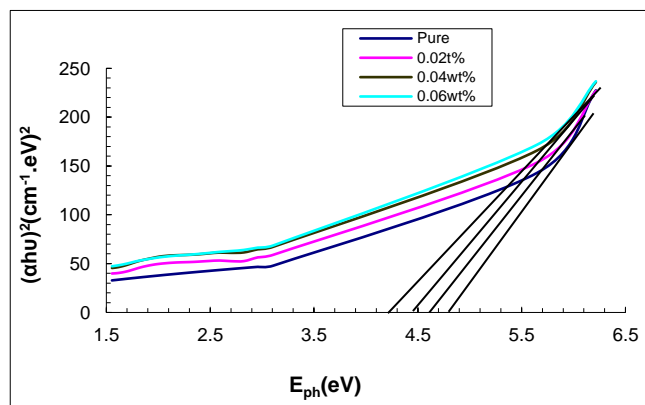
145

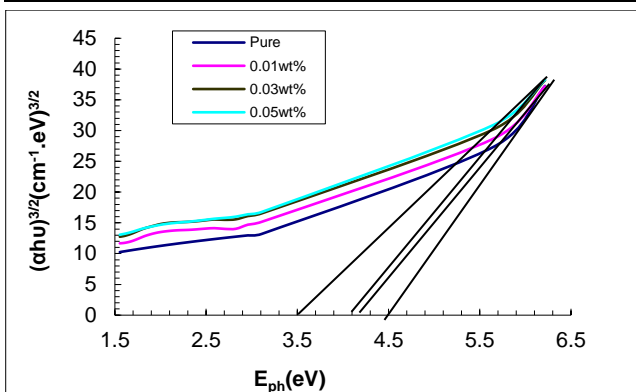**Fig. 4.** Energy gap values of permissible direct transitions

Fig. 5. Energy gap values of forbidden direct transitions.

The following table shows the energy gap values of permissible and forbidden direct transitions of the samples.

Sample	Permissible energy gap (ev)	forbidden energy gap (ev)
Pure	4.83	4.50
0.01 %	4.68	4.19
0.03 %	4.44	4.10
0.05 %	4.28	3.51

We note from the previous table that the values of energy band gap for permissible and forbidden electronic transitions decrease with the increase in the percentage of the doping, and this indicates that the width of local levels increased with increase in the percentage of the doping (Sahay et al, 2007; Dagdelen et al, 2012). The decreasing of energy band gap with increase of the doping ratios, which led to the inclination of the absorption edge towards lower energies, and consequently the decrease in the concentration of the charge carriers, and thus the value of the energy band gap decreased (Bakry and Mahmoud, 2011).

Refractive Index n_o

Give the complex refraction index by the formula:

$$\tilde{n} = n(\lambda) + iK(\lambda) \qquad (6)$$

Where real part (n) represents the refractive index and imaginary coefficient (k) is the damping coefficient. The damping is the amount of absorption energy in the material. The reflectivity formula (7) is given for the semiconductor in the orthogonal state of incidence (Zaid A. Hasan, 2019); (Bakry and Mahmoud, 2011):

$$R = \frac{(n-1)^2 + K^2}{(n+1)^2 + K^2} \qquad (7)$$

Knowing that the reflectivity on inner surface of the samples is neglected. By solving this equation, we arrive at the refractive index formula as follows (Yakuphanoglu et al, 2007; Chidi et al, 2008):

$$n = \left(\frac{1+R}{1-R}\right) + \sqrt{\frac{4R}{(1-R)^2} - K^2} \qquad (8)$$

$$\text{Where } K_o = \frac{\alpha\lambda}{4\pi} \qquad (9)$$

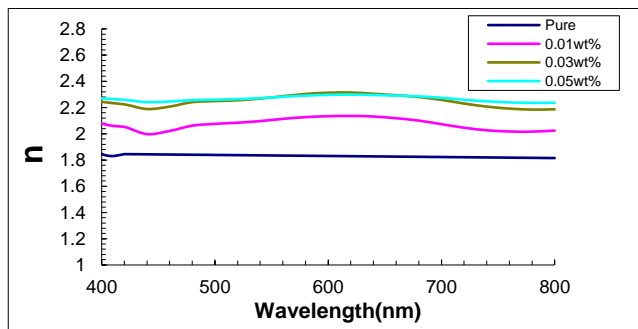The following figure shows the refractive index as function of wavelength.

Fig. 6. Changes the refractive index n_o in terms of the photon energy wavelength λ(nm) for films.

We note from the spectra of the refractive index that it increases with the increase in the percentage of doping, and a small peak appears at 600 nm approximately, in a pure sample, the spectrum is almost linear. The refractive index curve for all samples except the pure sample increases slightly with increasing wavelength (abnormal dispersion), and known that curve behavior of refractive index is almost similar to nature of the reflectivity due to correlation of R with n according to formula. (7). In addition, decreasing values of n at a wavelength bigger than 600 nm is due to decreasing absorption (Abdul Kader, 2018).

Extinction Coefficient K_o

The extinction coefficient (K) in terms of the absorption coefficient (α) has been calculated from the formula. (9). The following figure shows the extinction coefficient of prepared samples with wavelength:
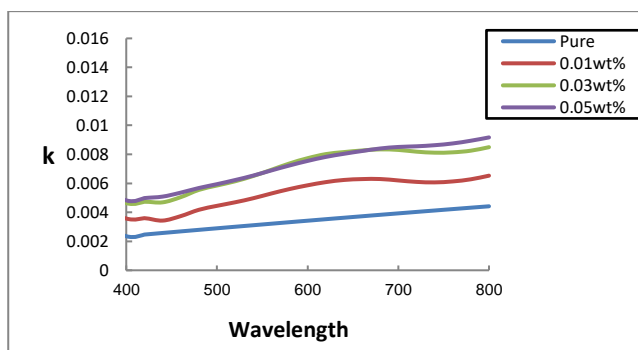

Fig. 7. Changes of extinction coefficient with wavelength λ(nm) for samples

146

The figure. 7 shows that the spectra of the extinction coefficient increase with the increase in doping ratios and are almost linear in pure sample, We found that the values of (k) are small in the case of low wavelengths and then begin to increase, and this indicates an increase in the absorption values and therefore an increase in the absorption coefficient according to the relationship (9) and the damping coefficient increases.

Dielectric Constant ε

Give the equation of complex dielectric constant is:
$$\tilde{\varepsilon} = \varepsilon_1 + i\varepsilon_2 = (n + ik)^2 = (n^2 - k^2) = i2nk \quad (10)$$
By separating the real and imaginary parts of the dielectric constant, we get the following two formulas (Mohamed et al, 2020; John, 1996):
$$\varepsilon_1 = n^2 - k^2 \qquad (11)$$
$$\varepsilon_2 = 2nk \qquad (12)$$
This depends on the absorption coefficient formula (3). The two figures (8,9) shows the spectra of the real and imaginary dielectric constants:
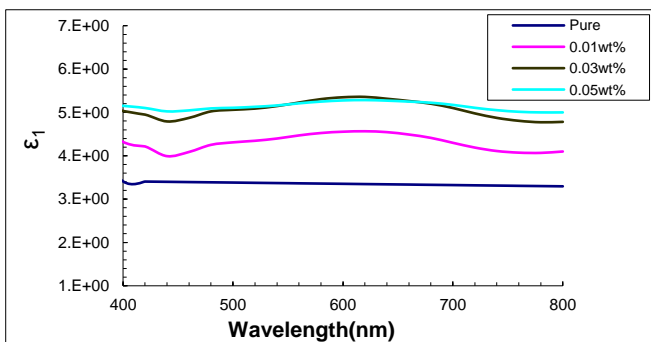

Fig. 8. Variations of real electrical dielectric constant εᵣ in terms of wavelength λ(nm) for films
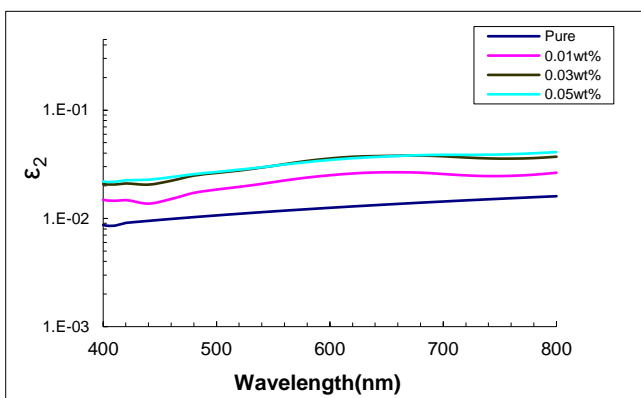

Fig. 9. Variations of the imaginary electrical dielectric constant εᵢ in terms of wavelength λ(nm) for films

It is clear from the curves of the real dielectric constant (Fig. 8) that they are similar to refractive index curves in (Fig. 6) because of their relationship

to the formula. (11) and in which the effect of extinction coefficient is weak.

As for Figure 9, it displays the spectra of the dummy dielectric constant of the motion of dipoles that cause energy loss, and we notice that the increase in impurities increases εᵢ and are almost similar when the dopant ratios 0.03 and 0.05.

Optical Conductivity σ_{op}

We have calculated the optical conductivity σ using the following equation (Ezema et al, 2004; Chidi et al 2007):
$$\alpha = \frac{4.\pi.\sigma}{n.c} \Rightarrow \sigma = \frac{\alpha.n.c}{4.\pi} \qquad (13)$$
Where: n: refractive index, c: light's speed, α: absorption coefficient. The following figure shows the optical conductivity as a function of wavelength:
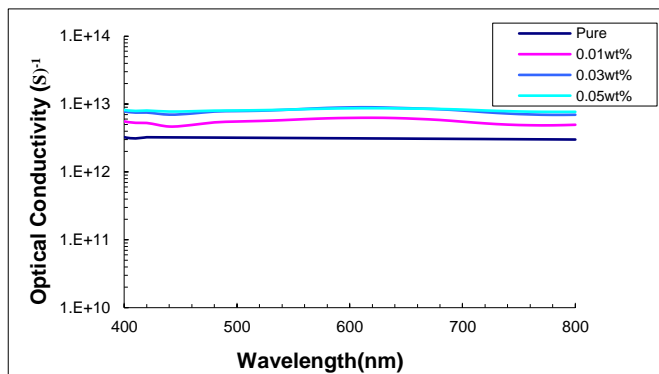

Fig. 10. Optical conductivity changes σ_{op} as function of $h\nu$ for samples

The previous figure shows that optical conductivity spectra increases when increase in percentage of doping, noting that two spectra of the doping ratios 0.03 and 0.05 are almost similar, where increase in optical conductivity is because increase charge carriers.

The behavior of optical conductivity is similar to behavior of the absorption coefficient α because the relationship between σ and α is a direct relationship and this is due to the fact that the greater the material's absorption of light, the majority and minority charge carriers are active in the movement and thus their number increases.

Conclusion

The drip and wipe method is a good and easy way to obtain a thin film, as the measurements were taken at room temperature in addition, normal atmospheric pressure without the need for vacuum. The impurity samples have good refractive index and dielectric constant, and they can also be used in applications with large n values. It was also found

that the transmittance decreases when the percentage of doping increases and therefore, the absorbance increases with the increase in the ratio at doping visible rays, which reached the highest peak at 600 nm almost. The real dielectric constant curves behave similar to the refractive index because they are related to each other where the damping coefficient is weak. On another hand, it was showing the energy band gap decreases with increase in the percentage of doping, and this increase led to the declinate of the absorption edges towards lower energies, that is, a decrease in the concentration of charge carriers.

References

Yadav AA, Barote MA, Masumdar EU. Studies on cadmium selenide (CdSe) thin films deposited by spray pyrolysis. *Materials Chemistry and Physics* 2010; 121(1-2): 53-57.

Bakry AM, Mahmoud SA. Effect of substrate temperature on the optical dispersion of sprayed nickel oxide thin films. *In Saudi International Electronics, Communications and Photonics Conference (SIECPC)* 2011: 1-7.

Jazmati AK, Abdallah B. Optical and structural study of ZnO thin films deposited by RF magnetron sputtering at different thicknesses: a comparison with single crystal. *Materials Research* 2018: 21(3).

Uhuegbu CC, Babatunde EB, Oluwafemi CO. The Study of Copper Zinc Sulphide (CuZnS_2) Thin Films. *Turkish Journal of Physics* 2008; 32(1): 39-47.

Dagdelen F, Serbetci Z, Gupta RK, Yakuphanoglu F. Preparation of nanostructured Bi-doped CdO thin films by sol–gel spin coating method. *Materials Letters* 2012; 80: 127-130.

Fernandez-Garcia M, Martinez-Arias A, Hanson JC, Rodriguez JA. Nanostructured oxides in chemistry: characterization and properties. *Chemical reviews* 2004; 104(9): 4063-4104.

Ezema FI. Optical characterization of chemical bath deposited bismuth oxyiodide (BiOI) thin films. *Turkish Journal of Physics* 2005; 29(2): 105-114.

Yang HS, Choi SY, Hyun SH, Park HH, Hong JK. Ambient-dried low dielectric SiO2 aerogel thin film. *Journal of Non-Crystalline Solids* 1997; 221(2-3): 151-156.

Habubi NF, Mishjal KH, Ziad TK. *Journal of College Education, AlMustansyriah University* 2002.

bo Zhong J, Zhang Li J, Mei Feng F, Lu Y, Zeng J, Hu W, Tang Z. Improved photocatalytic performance of SiO2–TiO2 prepared with the assistance of SDBS. *Journal of Molecular Catalysis A: Chemical* 2012; 357: 101-105.

Jassim JM, Khadim YH, Al-Sultani MMM. The study of a linear and non-linear optical property for PMMA thin films doped with the Rhodamine B laser dye and Ag nano particles are used in medicine. *Journal of Global Pharma Technology* 2017; 9(9): 207-2013.

John Wikey Sons, Inc. Chichester, Brisbane, Toronto, Singapore *Introduction to Solid State Physics*, New York 1996: 673.

Ghazaryan L, Sekman Y, Schröder S, Mühlig C, Stevanovic I, Botha R, Szeghalmi A. On the properties of nanoporous SiO2 films for single layer antireflection coating. *Advanced Engineering Materials* 2019: 21(6).

Liu S, Han MY. Silica-coated metal nanoparticles. *Chemistry–An Asian Journal* 2010; 5(1): 36-45.

Stylidi M, Kondarides DI, Verykios XE. Pathways of solar light-induced photocatalytic degradation of azo dyes in aqueous TiO2 suspensions. *Applied Catalysis B: Environmental* 2003; 40(4): 271-286.

Jayaraj MK, Antony A, Ramachandran M. Transparent conducting zinc oxide thin film prepared by off-axis rf magnetron sputtering. *Bulletin of Materials Science* 2002; 25(3), 227-230.

Hassen M, Riahi R, Laatar F, Ezzaouia H. Optical and surface properties of CdSe thin films prepared by sol-gel spin coating method. *Surfaces and Interfaces* 2020: 18.

Ghobadi N, Sohrabi P, Hatami HR. Correlation between the photocatalytic activity of CdSe nanostructured thin films with optical band gap and Urbach energy. *Chemical Physics* 2020: 538.

Kissinger NJ, Kumar JSB, Balasubramaniam T, Perumal K. Effect of substrate temperature on the structural and optical properties of nanocrystalline cadmium selenide thin films prepared by electron beam evaporation technique. *Acta Physica Polonica A* 2010; 118(4): 623-628.

Sahay PP, Nath RK, Tewari S. Optical properties of thermally evaporated CdS thin films. Crystal Research and Technology: *Journal of Experimental and Industrial Crystallography* 2007; 42(3): 275-280.

Ardalan RB, Jamshidi N, Arabameri H, Joshaghani A, Mehrinejad M, Sharafi P. Enhancing the permeability and abrasion resistance of concrete using colloidal nano-SiO2 oxide and spraying nanosilicon practices. *Construction and Building Materials* 2017; 146: 128-135.

Vishwakarma SR, Kumar A, Prasad S, Tripathi RSN. Synthesis and Characterization of n-CdSe Thin Films Deposited at different Substrate Temperatures. *Chalcogenide Letters* 2013: 10(10).

Maekawa S, Ohishi T. Evaluation of SiO2 thin films prepared by sol-gel method using photoirradiation. *Journal of non-crystalline solids* 1994; 169(1-2): 207-209.

Venkatachalam S, Mangalaraj D, Narayandass SK. Structural, optical properties and VCNR mechanisms in vacuum evaporated iodine doped ZnSe thin films. *Applied Surface Science* 2007; 253(11): 5137-5142.

Sietsma JR, Meeldijk JD, den Breejen JP, Versluijs-Helder M, Van Dillen AJ, de Jongh PE, de Jong KP. The preparation of supported NiO and Co3O4 nanoparticles by the nitric oxide controlled thermal decomposition of nitrates. *Angewandte Chemie International Edition* 2007; 46(24): 4547-4549.

Srivastava AK. *Oxide Nanostructures, Growth, Macrostructures and Properties;* Pan Stanford Publishing: Singapore, 2014.

Gholami T, Bazarganipour M, Salavati-Niasari M, Bagheri S. Photocatalytic degradation of methylene blue on TiO2@ SiO2 core/shell nanoparticles: synthesis and characterization. *Journal of Materials Science: Materials in Electronics* 2015; 26(8): 6170-6177.

Ha TJ, Park HH, Jang HW, Yoon SJ, Shin S, Cho HH. Study on the thermal stability of ordered mesoporous SiO2 film for thermal insulating film. *Microporous and mesoporous materials* 2012; 158: 123-128.

Jia-Jin T, Yan C, Wen-Jun Z, Qing-Quan G. Elastic and thermodynamic properties of CdSe from first-principles calculations. *Communications in Theoretical Physics* 2008; 50(1): 220-226.

Alwan TJ. Refractive index dispersion and optical properties of dye doped polystyrene films. *Malaysian polymer journal* 2010; 5(2): 204-213.

Yakuphanoglu F, Kandaz M, Yaraşır MN, Şenkal FB. Electrical transport and optical properties of an organic semiconductor based on phthalocyanine. *Physica B: Condensed Matter* 2007; 393(1-2): 235-238.

Hasan ZA. Effect Magneto–Optic on Ferromagnetic Nanoparticle Polymer Composite Films. *NeuroQuantology* 2021; 19(6): 25-29.

Hasan ZA. Study the effect of magnetic field on polymer doping Tio2 nanoparticles. *NeuroQuantology* 2019; 17(12): 39-43.